Scientific Research Publishing

Open Journal of Modelling and Simulation, 2026, 14(2), 45-62
https://www.scirp.org/journal/ojmsi
ISSN Online: 2327-4026
ISSN Print: 2327-4018

Operating Patterns and Reaction Mechanism of Propane Pyrolysis Pathway

Zheng Wu, Hui Fang, Rui-Shen Xie, Mei-Feng Chen, Qian-Feng Zhang*

School of Materials Science and Engineering, Institute of Molecular Engineering and Applied Chemistry, Anhui University of Technology, Ma'anshan, China
Email: *zhangqf@ahut.edu.cn

How to cite this paper: Wu, Z., Fang, H., Xie, R.-S., Chen, M.-F. and Zhang, Q.-F. (2026) Operating Patterns and Reaction Mechanism of Propane Pyrolysis Pathway. *Open Journal of Modelling and Simulation*, **14**, 45-62.
https://doi.org/10.4236/ojmsi.2026.142003

Received: January 13, 2026
Accepted: February 11, 2026
Published: February 14, 2026

Abstract

In the context of the accelerated transition of the global energy structure to decarbonization, propane is not only rich in reserves but also has a low carbon-to-hydrogen ratio, which is a natural advantage for the production of high-value-added chemicals (e.g., ethylene and propylene) through efficient conversion. This study employs the M06-2X/6-31++G(d,p) density functional theory method combined with transition state theory to calculate the energy barriers for each radical reaction involved in propane pyrolysis. The results indicate that in the initial reaction, the dissociation energy of the propane C-C bond is lower than that of the C-H bond, confirming that symmetrical cleavage of the C-C bond is the dominant initiation pathway in the early stages of pyrolysis. Based on the principles of radical chain reactions, four core pyrolysis reaction pathways were designed, with a focus on comparing the energy characteristics of propylene and ethylene formation: Path 1 and 2 utilize primary propyl radicals (n-C_3H_7•/i-C_3H_7•) as active centers, with ethylene formation energy barriers of 136.83 kcal/mol and propylene formation energy barriers of 145.98 kcal/mol; Path 3 and 4 introduce secondary radicals (C_2H_5•) to participate in chain transfer, the formation energy barrier of ethylene is 120.87 - 174.8 kcal/mol, and that of propylene is 124.79 - 174.8 kcal/mol; This study reveals the core mechanism for selectively controlling propylene and ethylene production by comparing bond dissociation energy patterns with pathway energies. It provides critical theoretical foundations for optimizing cracking process parameters and catalyst design, thereby supporting the chemical industry's transition toward low-carbon and high-efficiency operations.

Keywords

Propane, Pyrolysis, Reaction Pathway, Reaction Mechanism, Transition

State, Energy, Calculational Chemistry

1. Introduction

The demand for ethylene and propylene continues to expand as core raw materials for the modern chemical industry, and they are widely used in the production of high-value-added products such as polyethylene, polypropylene and propylene oxide. Currently, most of our ethylene and propylene are prepared by hydrocarbon pyrolysis processes, and the chemical utilization of alkanes for the production of valuable chemicals has become particularly attractive [1]-[3]. Among them, low-carbon alkanes such as propane are regarded as ideal feedstocks to replace traditional petroleum cracking due to their abundant reserves and high hydrogen-to-carbon ratio.

Conventional alkane conversion processes (e.g., steam cracking [4], oxidative dehydrogenation [5]-[7], catalytic dehydrogenation [8] [9]) can achieve olefin production, but face three challenges for industrial application: 1) High energy intensity due to high temperature operation, accompanied by large amount of CO_2 emission; 2) Low selectivity of target products due to the competition of multiple paths in the free-radical chain reaction, and low separation cost due to the formation of by-products of methane and hydrogen and carbon accumulation; 3) The problem of catalyst carbon deactivation and reactor coking significantly shortens the operating cycle.

These problems can be partially mitigated by novel reactor designs, catalyst modifications, and in situ spectroscopic techniques such as FTIR. Using propane as the primary feedstock, the researchers used a detailed gas-phase mechanistic model and a piston reactor model to evaluate reactor performance with respect to parameters such as inlet temperature, argon addition, and co-feeding of propane with oxygen, water, and carbon dioxide [10]. Meanwhile, propane oxidation in supercritical water was investigated under isothermal and isobaric conditions using a batch reactor facility, and it was found that increasing the temperature from 375˚C to 400˚C at 220 bar increased propylene production and suppressed acetone generation, while increasing the pressure from 220 bar to 400 bar at 375˚C suppressed propylene, ethylene, and acetone generation and increased methane production [11]. In terms of catalyst modification, Fe/ZSM-5 catalysts were synthesized by combining Fe with ZSM-5 at different loadings. XRD and FT-IR characterization showed that the modified catalysts retained their crystallinity after metal impregnation, and the introduction of Fe into ZSM-5 improved the ethylene selectivity [12]. The Ga-modified HZSM-5 catalyst was used for the dehydroaromatization of propane and showed excellent reaction performance [13]. The reaction involves the dehydrogenation of propane to propylene and further formation of aromatics through polymerization, cyclization and dehydrogenation. However, the bifunctional catalysts are difficult to apply on a large scale due

to the high preparation cost. In addition, boron in the form of nanosheets was employed as a catalyst for the efficient oxidative dehydrogenation of propane, and the transformation of boron nanosheets into a thermally stable structure during the reaction was confirmed by TG-MS, FT-IR and XRD techniques [14]. The B-O/B-OH sites are the active centers of the reaction, and the catalyst can improve the selectivity of propylene and ethylene.

Fundamentally, the root of the above bottlenecks lies in the insufficient knowledge of the microscopic reaction mechanism of alkane pyrolysis, especially the breaking paths of the C-C and C-H bonds, the chain transfer behaviors of transient radicals, and the side reactions in the pyrolysis process. The synergistic application of theoretical simulation methods (e.g., ReaxFF molecular dynamics) provides a new perspective to reveal the atomic-scale mechanisms of pyrolysis reactions.

In the field of alkane reaction simulation research, new simulation methods and techniques continue to emerge. Researchers have developed a new reaction ReaxFF force field (2023-Pt/C/H) to simulate the Pt surface-catalyzed propane dehydrogenation reaction on a large scale, and successfully simulated the formation process of propylene in the gas phase, as well as the competing reaction scenarios generated by H and C [15]. The reaction ReaxFF force field has been used in the simulation of propane dehydrogenation on a large scale. The pyrolysis mechanism of *n*-decane and its isomers was investigated by the ReaxFF molecular dynamics method, and the effects of isomerization on the initial pyrolysis pathways and the formation of major products of straight-chain alkanes were evaluated. It was found that the initial pyrolysis of *n*-decane and its isomers at high temperatures mainly proceeded through the cleavage of the C-C and C-H bonds at different positions, and that the branched methyl group and the shortened carbon chain significantly affected the product distribution [16]. At the same time, the recently developed neural network atomic potential was used to carry out large-scale accurate reaction kinetics simulations, and the complex reaction network was sorted out in the form of a hierarchical network, so as to elucidate the key features of the oxidative dehydrogenation mechanism of light alkanes [17].

Based on this, first, the bond dissociation energies of the initial reactions of propane pyrolysis are calculated and their carbon and hydrogen bond-breaking capacities are initially analyzed. Second, the activation energy data of each radical reaction involved in propane pyrolysis are simulated and analyzed. Finally, the simulated activation energy data are plotted as energy barrier diagrams to qualitatively analyze the main reaction pathways of propane pyrolysis to ethylene and propylene.

2. Experimental and Method

2.1. Experimental Procedure

Pyrolysis gas products from hexane were analyzed using Py-GC/MS coupling technology. Hexane served as a model compound to replace gaseous propane, in-

directly validating the propane pyrolysis mechanism. A 5 μL aliquot of analytical-grade liquid hexane (purity ≥ 99.5%) was placed in a quartz pyrolysis tube. Inert quartz wool was used for fixation and sealing to prevent sample volatilization. After sealing, the tube was purged with nitrogen gas (flow rate 50 mL/min) for 3 minutes to remove oxygen. Heat at a rate of 10˚C/min to the target pyrolysis temperature of 800˚C, then hold at this temperature to complete pyrolysis. The gaseous products generated during pyrolysis were introduced into the gas chromatograph. Chromatographic separation and mass spectrometry enable qualitative and quantitative analysis of product composition, providing experimental data to support investigations into pyrolysis reaction pathways and selective control mechanisms.

2.2. Computational Method

With the support of GaussView software, Gaussian software can be applied in related fields such as chemistry, biochemistry, and physical chemistry [18]-[21]. Gaussian software calculates chemistry using two main methods: molecular mechanics methods and electronic structure theory, which in turn includes semi-empirical methods, *ab* initio calculations, and density-functional theory methods [22]. The M062X/6-31++G(d,p) level of calculation has been shown to give accurate thermodynamic properties and potential heights for hydrocarbons [23]-[26].

In this paper, the M06-2X/6-31++G(d,p) method was used to optimize the geometries of the reactants and products involved in the starting reaction, and all optimized structures were subjected to vibrational analysis by frequency calculations, which determined that there were no imaginary frequencies for either the reactants or the products. Transition states were identified using the Transition State (TS) method, ensuring that each transition state structure possesses only one imaginary frequency. Furthermore, each reaction underwent Intrinsic Reaction Coordinate (IRC) validation to ensure an accurate connection between reactants and products at every transition state.

All reaction path calculations were computationally realized using the G09W software with the implemented "strict" convergence criteria and "ultra-fine" integration grid. **Figure 1** shows the optimized geometry of the species involved in the initial decomposition of propane.

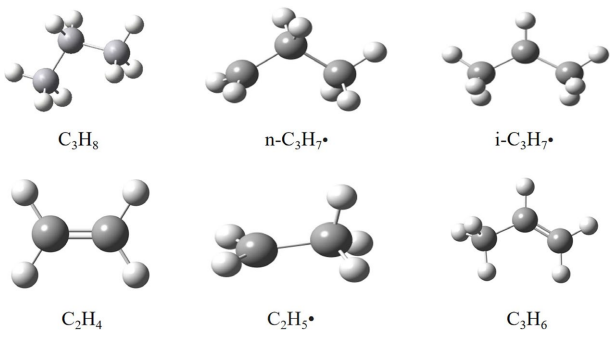

Figure 1. The optimized geometry of the species involved in the initial decomposition of propane.

3. Results and Discussion

3.1. Product Distribution Analysis of Hexane Pyrolysis

Since propane is a gas, making experimental control challenging, we supplemented the experiment with a pyrolysis study of hexane (another alkane with a representative structure). This indirectly validated the core conclusion that the primary products of alkane pyrolysis are olefins.

Tables 1-3 present the product distributions from three experimental pyrolysis studies of hexane. Based on the alkane radical chain pyrolysis mechanism, the validity of propane pyrolysis energy calculations is validated using hexane (an alkane homologue) pyrolysis products: The tabulated data indicate that the initial stage of hexane pyrolysis is a "primary cracking phase" dominated by radical chain reactions: The C-C bonds in the feedstock hexane undergo low-energy-barrier cleavage, yielding small-molecule alkanes and alkenes. At this stage, alkenes constitute a high proportion and are one of the primary products in the early pyrolysis phase. The later stage is the "product evolution phase" dominated by secondary reactions of the alkenes: The initially formed alkenes undergo secondary reactions such as hydrogenation and addition (e.g., alkenes reacting with radicals to form alkanes), leading to a significant decrease in the proportion of alkenes, while small-molecule alkanes become the dominant products. This temporal product evolution closely aligns with the reaction pathway derived from propane pyrolysis energy barriers, indirectly validating the reliability of propane pyrolysis energy calculations and providing experimental support for the rationality of the propane pyrolysis reaction mechanism.

Hexane was selected as the model compound to validate the propane pyrolysis mechanism, primarily based on the fact that homologous series of alkanes undergo pyrolysis via a unified radical chain reaction mechanism. Specifically, all undergo C-C/C-H bond cleavage to generate radicals, followed by chain propagation through β-scission and hydrogen abstraction reactions, ultimately yielding small-molecule alkanes and alkenes. This commonality provides a robust theoretical foundation for analogical validation. The core reaction pathways and radical evolution patterns of low-carbon alkanes (C3-C6) pyrolysis exhibit high consistency. Minor differences in energy barriers due to carbon chain length do not compromise the validity of the mechanism correlation.

The kinetics of the two processes exhibit distinct differences in cage effects. The gas-phase pyrolysis of C3 propane shows no cage effect, with reaction rates primarily governed by molecular diffusion and collision frequency. In contrast, the cage effect during liquid-phase pyrolysis of C6 hexane slightly increases radical recombination probability, though this effect is significantly weakened at elevated temperatures. By precisely correlating the temporal distribution of hexane pyrolysis products with the radical reaction patterns of propane pyrolysis, this study effectively addresses the challenge of direct detection in gaseous propane and enhances the scientific rigor of mechanism validation.

Table 1. Product distribution of hexane pyrolysis experiment 1.

Entry	Methane %	Ethane %	Ethylene %	Propane %	Propylene %	*i*-Butane %	*n*-Butane %	*trans*-Butene %	Butene-1%	*i*-Butylene %	cis-Butylene %	C5-%	H_2
1	23.04	1.98	10.2	0.08	2.3	0.33	60.62	0.24	0.1	0.06	0.18	0.87	/
2	31.57	2.54	12.14	0.09	2.57	0.26	49.34	0.21	0.1	0.05	0.15	0.98	/
3	29.78	1.92	12.86	0.08	2.67	0.32	50.84	0.21	0.11	0.06	0.14	1.01	46.14
4	30.44	1.92	13	0.08	2.72	0.3	50.16	0.2	0.11	0.05	0.14	0.88	47.17
5	27.78	1.98	13.3	0.08	2.87	0.33	52.54	0.22	0.12	0.06	0.16	0.56	48.36
6	29.33	1.88	12.37	0.07	2.57	0.31	52.14	0.21	0.11	0.06	0.14	0.81	49.2
7	24.82	1.84	12.12	0.07	2.66	0.35	56.19	0.23	0.11	0.06	0.16	1.39	50.15
8	24.42	1.84	11.95	0.07	2.61	0.37	57.48	0.24	0.10	0.06	0.16	0.70	50.71
9	24.79	1.77	11.2	0.07	2.36	0.35	57.94	0.23	0.10	0.06	0.16	0.97	50.7
10	19.22	1.75	10.61	0.07	2.40	0.38	64.14	0.26	0.10	0.07	0.18	0.82	45.08

Table 2. Product distribution of hexane pyrolysis experiment 2.

Entry	Methane %	Ethane %	Ethylene %	Propane %	Propylene %	*i*-Butane %	*n*-Butane %	*trans*-Butene %	Butene-1 %	*i*-Butylene %	*cis*-Butylene %	C5-%	H_2
1	15.86	1.55	11.55	0.08	2.87	0.43	65.57	0.29	0.13	0.07	0.21	1.39	44.46
2	16.38	1.72	12.09	0.16	2.94	0.41	64.32	0.29	0.12	0.08	0.20	1.29	45.46
3	20.41	1.85	12.50	0.09	3.03	0.39	59.56	0.28	0.13	0.08	0.19	1.49	45.16
4	18.01	1.79	12.11	0.08	2.93	0.39	62.35	0.27	0.11	0.07	0.19	1.70	41.97
5	22.27	1.98	12.89	0.09	3.17	0.37	56.77	0.26	0.14	0.07	0.19	1.80	42.66
6	23.04	2.04	13.22	0.67	3.26	0.37	54.74	0.27	0.14	0.11	0.19	1.95	41.85
7	21.83	2.11	13.97	0.20	3.45	0.36	55.98	0.25	0.13	0.07	0.17	1.48	39.76
8	24.11	2.13	13.57	0.09	3.35	0.36	54.01	0.25	0.13	0.07	0.17	1.76	38.52
9	22.05	2.15	14.14	0.10	3.52	0.35	55.22	0.25	0.13	0.07	0.17	1.85	37.77
10	21.61	2.12	13.96	0.10	3.51	0.36	56.07	0.26	0.14	0.07	0.18	1.62	36.52

Table 3. Product distribution of hexane pyrolysis experiment 3.

Entry	Methane %	Ethane %	Ethylene %	Propane %	Propylene %	*i*-Butane %	*n*-Butane %	*trans*-Butene %	Butene-1 %	*i*-Butylene %	*cis*-Butylene %	C5-%	H_2
1	19.45	1.23	17.82	0.1	2.83	0.33	52.64	0.26	0.2	0.07	0.18	4.89	47.04
2	23.41	2.3	30.15	0.25	6.46	0.18	28.02	0.2	0.44	0.09	0.15	8.35	37.82
3	19.85	3.52	30.71	0.41	12.35	0.18	25.57	0.27	0.96	0.17	0.21	5.8	23.7
4	5.94	0.45	4.32	0.08	1.49	0.54	83.92	0.39	0.16	0.08	0.28	2.36	/
5	1.79	0.43	3.04	0.05	2.05	0.58	90.46	0.37	0.17	0.08	0.25	0.73	4.96
6	2.23	0.5	3.20	0.05	2.28	0.66	89.28	0.42	0.19	0.09	0.29	0.81	4.61
7	1.93	0.45	2.70	0.05	2.07	0.68	90.64	0.42	0.18	0.08	0.29	0.51	3.87
8	1.31	0.34	2.03	0.04	1.65	0.59	92.62	0.37	0.15	0.07	0.25	0.58	3.36
9	1.48	0.36	2.02	0.03	1.62	0.66	92.48	0.41	0.15	0.08	0.28	0.43	2.85
10	1.01	0.28	1.52	0.04	1.28	0.58	94.01	0.37	0.12	0.07	0.25	0.47	2.45

3.2. Initial Reactions of Propane Pyrolysis

To determine the pyrolysis mechanism of propane, it is necessary to study the initial reactions of propane pyrolysis. The bond dissociation energy is an important reference for judging the ease of bond breaking; the larger the bond dissociation energy the less likely it is to break, and vice versa [27]. In terms of computational accuracy, the M06-2X functional demonstrates outstanding performance in calculating the thermochemical properties of alkanes, with its predicted bond dissociation energy errors typically ≤ 2% [28]. The 6-31++G(d,p) basis set, incorporating diffusion and polarization functions, effectively describes the electron distribution in radical systems.

Figure 2 shows the calculated bond dissociation energies for the three initial pyrolysis pathways of the propane molecule. The C-C bond dissociation energy of 95.587 kcal/mol obtained in this study is slightly higher than values reported in other literature [29] [30]. However, it falls within the reasonable fluctuation range of calculations using different DFT methods, with the discrepancy primarily stemming from differences in how the functional describes electron correlation effects. The bond dissociation energy of secondary C-H bonds (104.672 kcal/mol) in this study is lower than that of primary C-H bonds (108.069 kcal/mol). This aligns with the general principle that "secondary carbon free radicals exhibit greater stability due to hyperconjugation, resulting in lower corresponding bond dissociation energies" [31] [32]. The bond dissociation energy for the C-C bond is lower than that for the C-H bond. Therefore, Path 3 is the kinetically optimal path and is the most likely to occur in the initiation reaction.

Numerical discrepancies arising from different theoretical approaches are normal phenomena. The findings of this study do not contradict the core consensus in the literature: C-C bond dissociation energies are lower than C-H bonds, and secondary C-H bonds exhibit lower dissociation energies than primary C-H bonds. The methodological choices are based on clear scientific rationale, and the computational data provide a foundation for the future development of alkane pyrolysis technology.

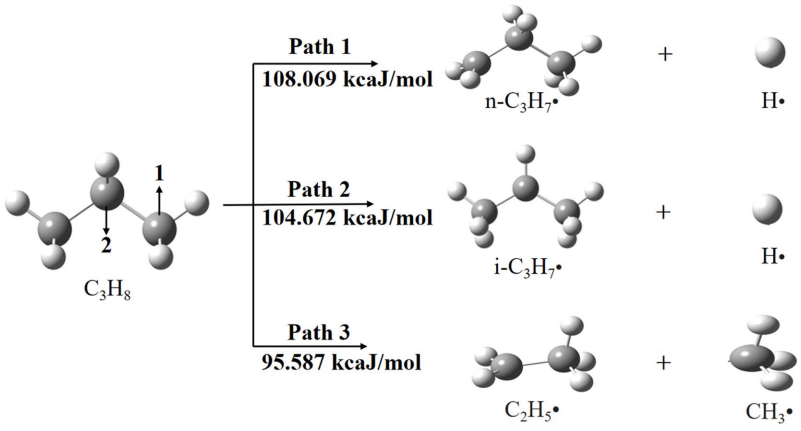

Figure 2. Initial reaction path of propane pyrolysis.

3.3. Free Radical Reactions of Propane Pyrolysis

From the experiments, the main products of propane pyrolysis are ethylene, propylene, hydrogen, methane and ethane [33] [34]. The reaction pathways are significantly affected by radical stability and reaction conditions. For example, high temperatures may promote homocleavage (initiation phase) and β-breakage (transfer phase), increasing the proportion of ethylene [35]. Low temperatures may inhibit C-C bond breaking and promote C-H bond breaking to generate H- and propyl radicals. And low pressure reduces the probability of radical collision, decreases the termination reaction rate, extends the chain reaction lifetime, and enhances the main product selectivity.

Table 4 shows the various radical reactions involved in the pyrolysis of propane. Pyrolysis typically involves a free radical chain reaction consisting of three phases: initiation, transfer, and termination [36]. In the initiation phase, the propane molecule is homolyzed to generate the initial radicals. In the transfer stage, each radical reacts with the propane molecule to form products and regenerate radicals, maintaining the chain cycle. In the termination phase, the termination reaction usually requires a high concentration of radicals to occur, and its rate directly affects the duration and product selectivity of the chain reaction. The transition state structures involved in the free radical reactions 4, 5, 6...14 are named TS_4, TS_5, TS_6...TS_{14}, as shown in Figure 3.

Table 4. Free radical reactions of propane pyrolysis.

Reaction type	Reaction number	Free radical reaction
Chain initiation	1	$C_3H_8 \rightarrow n\text{-}C_3H_7\bullet + H\bullet$
	2	$C_3H_8 \rightarrow i\text{-}C_3H_7\bullet + H\bullet$
	3	$C_3H_8 \rightarrow C_2H_5\bullet + CH_3\bullet$
	4	$C_2H_5\bullet \rightarrow C_2H_4 + H\bullet$
	5	$n\text{-}C_3H_7\bullet \rightarrow C_3H_6 + H\bullet$
	6	$i\text{-}C_3H_7\bullet \rightarrow C_3H_6 + H\bullet$
	7	$n\text{-}C_3H_7\bullet \rightarrow C_2H_4 + CH_3\bullet$
	8	$i\text{-}C_3H_7\bullet \rightarrow n\text{-}C_3H_7\bullet$
Chain transfer	9	$CH_3\bullet + C_3H_8 \rightarrow n\text{-}C_3H_7\bullet + CH_4$
	10	$CH_3\bullet + C_3H_8 \rightarrow i\text{-}C_3H_7\bullet + CH_4$
	11	$C_2H_5\bullet + C_3H_8 \rightarrow n\text{-}C_3H_7\bullet + C_2H_6$
	12	$C_2H_5\bullet + C_3H_8 \rightarrow i\text{-}C_3H_7\bullet + C_2H_6$
	13	$H\bullet + C_3H_8 \rightarrow n\text{-}C_3H_7\bullet + H_2$
	14	$H\bullet + C_3H_8 \rightarrow i\text{-}C_3H_7\bullet + H_2$
Chain cessation	15	$H\bullet + H\bullet = H_2$
	16	$H\bullet + CH_3\bullet = CH_4$

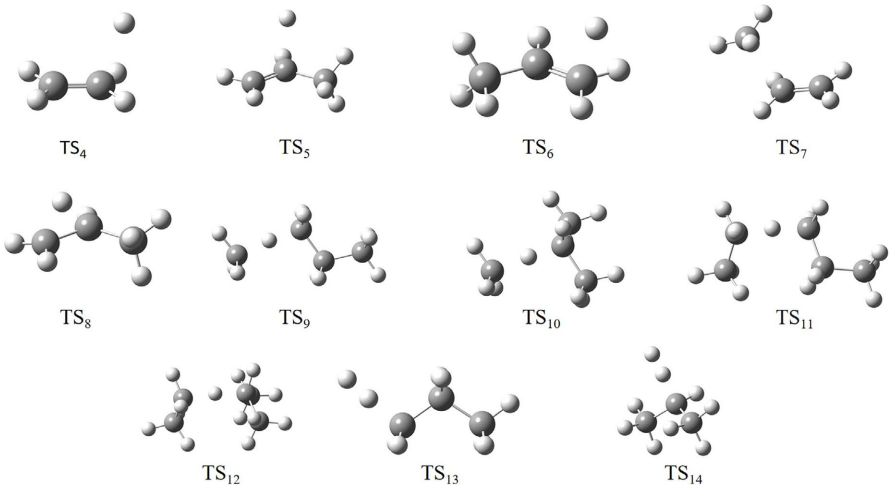

Figure 3. Transition state geometry involved in each free radical reaction.

3.4. Reaction Path Design and Calculation for Propane Pyrolysis

Based on the free radical reaction mechanism of propane pyrolysis, four possible reaction paths were analyzed and organized for the formation of the products ethylene and propylene.

As shown in Figure 4 and Figure 5, Pathways 1 and 2 are reactions initiated by C-H bond cleavage. Experimental results from propane pyrolysis indicate that the primary products are propylene, ethylene, hydrogen, and methane. The initial step involves C-H bond cleavage: Path 1 forms *n*-C_3H_7•, while Path 2 forms *i*-C_3H_7•. In pathway 1, *n*-C_3H_7• generates methane via steps 7 and 9, and produces H_2 via steps 5 and 13. In pathway 2, *i*-C_3H_7• yields corresponding products via steps 8 and 10, and steps 6 and 14. The structural difference between *n*- and *i*-propyl radicals leads to distinct product ratios along the two pathways. This represents the proposed reaction pathways for propane's primary olefin products. For other products, given their minor contributions, predicting their formation would be extremely complex and challenging; thus, this is not pursued here.

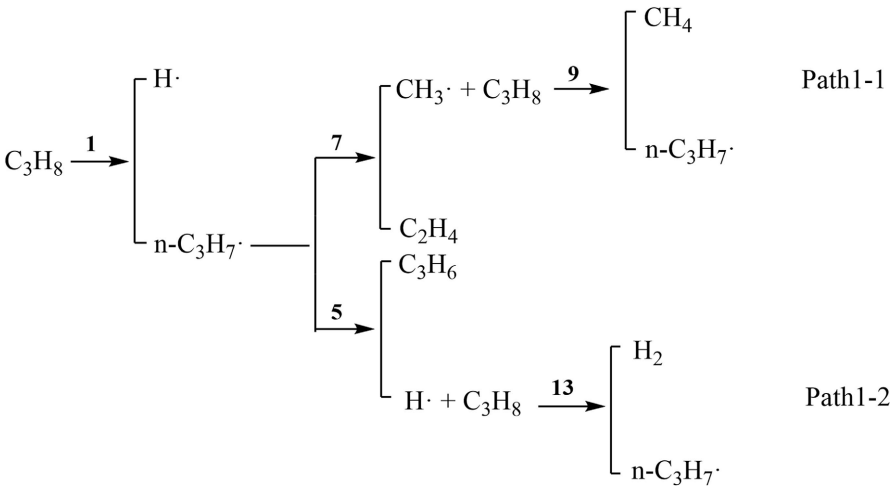

Figure 4. Design of propane pyrolysis path 1.

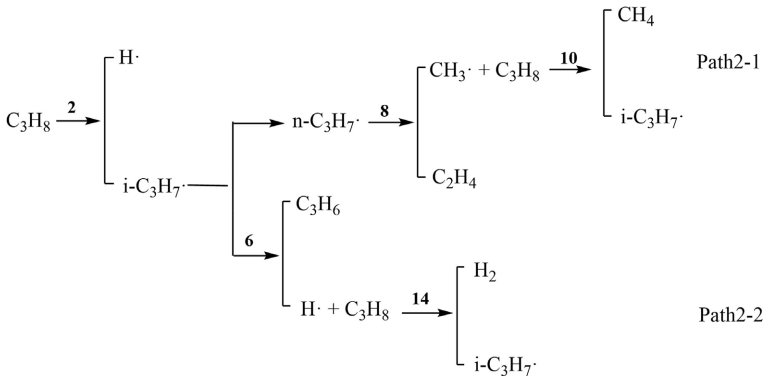

Figure 5. Design of propane pyrolysis path 2.

After inferring the pyrolysis pathway of propane based on its product distribution, it is necessary to calculate the reaction energy barrier pathway to validate its feasibility. The energy barrier diagrams for propane pyrolysis Path 1 and Path 2 are shown in Figure 6 and Figure 7, respectively, clearly illustrating the energy level differences among the reactions.

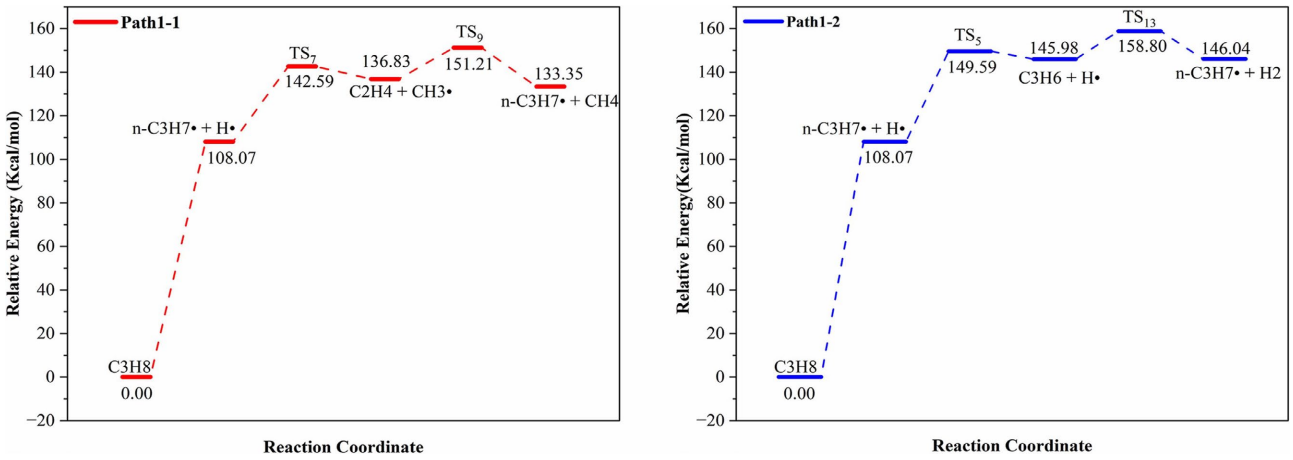

Figure 6. Schematic representation of the reaction energy barriers during the formation of ethylene and propylene in path 1.

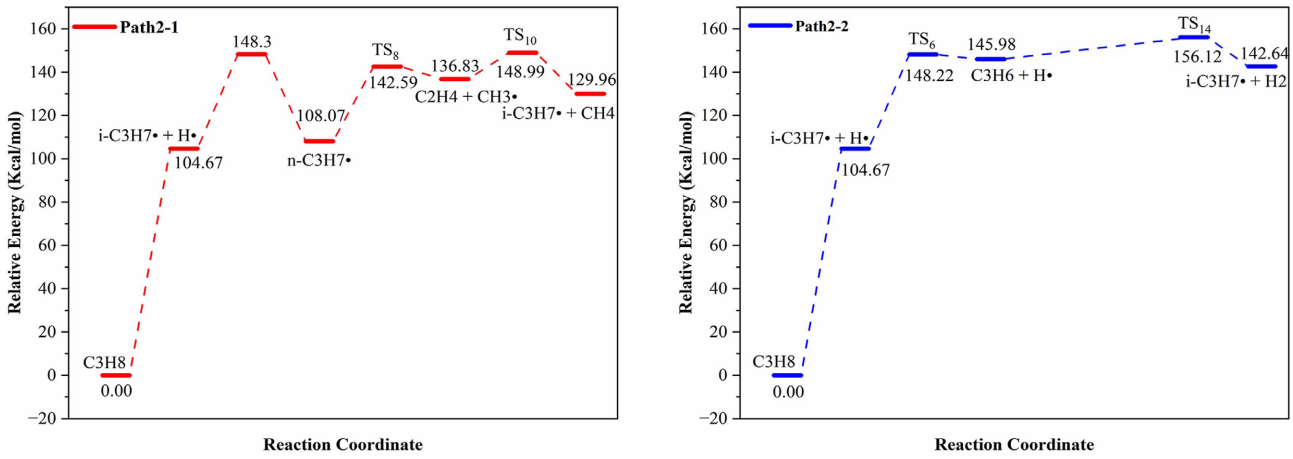

Figure 7. Schematic of the reaction energy barriers during the formation of ethylene and propylene in path 2.

The energy barrier difference between propane pyrolysis Path 1 and Path 2 fundamentally stems from the distinct properties of radical structures and reaction bonds. During the initial C-H bond cleavage stage, Path 2 exhibits a lower energy barrier (104.67 kcal/mol) than Path 1 (108.07 kcal/mol). This arises because the isopropyl radical possesses a stronger hyperconjugation effect and a more dispersed electron cloud, which weakens the bond energy of the initial C-H bond, making it easier to break.

The difference in product energy barriers is directly related to the bond types involved in the reaction. The energy barrier for ethylene formation (approximately 142.59 kcal/mol) is nearly identical for both pathways because the corresponding β-cleavage involves a terminal C-C bond. This bond exhibits uniform electron density distribution and no significant side-chain disturbance affecting its bond energy. In contrast, the energy barrier for propylene formation (Path 1: 149.59 kcal/mol; Path 2: 148.22 kcal/mol) is higher. This is because the corresponding C-C bond is adjacent to a side chain, where the hyperconjugation effect stabilizes the bond, increasing the energy required for cleavage. Comparatively, ethylene has a slightly lower energy barrier, making its formation more favorable during the initial stages of pyrolysis. Among other products, the energy barriers for CH_4 (Path 1: 151.21 kcal/mol; Path 2: 148.99 kcal/mol) are lower than those for H_2 (Path 1: 158.80 kcal/mol; Path 2: 156.12 kcal/mol). This stems from CH_4 formation involving radical hydrogen abstraction (single bond transfer, requiring lower energy barriers), whereas H_2 formation involves dehydrogenation (involving double electron pair bond breaking, consuming more bond energy). Thus, the alkane product CH_4 forms earlier than H_2.

From the pyrolysis mechanism perspective, the structural differences of initial radicals determine pathway initiation ease, while the height of product energy barriers directly corresponds to formation timing. Ethylene (low energy barrier) accumulates initially, while propylene and CH_4 (medium energy barrier) increase as the reaction progresses. H_2 (high energy barrier) gains a larger proportion in the later stages. These energy barrier differences clearly illustrate pyrolysis patterns: the energy level differences in the energy barrier diagram directly reflect reaction priority, fundamentally embodying the pyrolysis principle that "the lower the energy barrier, the earlier the product forms".

As shown in **Figure 8** and **Figure 9**, pathways 3 and 4 are reactions triggered by C-C bond cleavage. Path 3 initiates with the initial C-C bond cleavage of propane (distinct from the C-H cleavage in Paths 1 and 2), generating two types of radicals: CH_3• and C_2H_5•. After conversion to *n*-C_3H_7• via hydrogen abstraction reactions (Steps 9, 11, 13), β-cleavage (Step 7) and dehydrogenation (Step 5) concurrently yield CH_4, C_2H_4, and C_3H_6. This pathway centers on multi-radical product evolution driven by carbon-carbon bond cleavage. Pathway 4 features *i*-C_3H_7• as its core radical. Due to the insufficient terminal carbon chain length of this branched radical, direct ethylene formation via β-cleavage is unfeasible. Therefore, only the energy barrier for propylene generation was calculated: *i*-C_3H_7• undergoes dehydro-

genation in Step 6 to form C_3H_6. Pathways 4-1 to 4-3 all focus on propylene production, demonstrating how the structural properties of branched radicals limit product formation. This contrasts with the multi-product pathways of Pathway 3, reflecting structurally driven evolutionary differences.

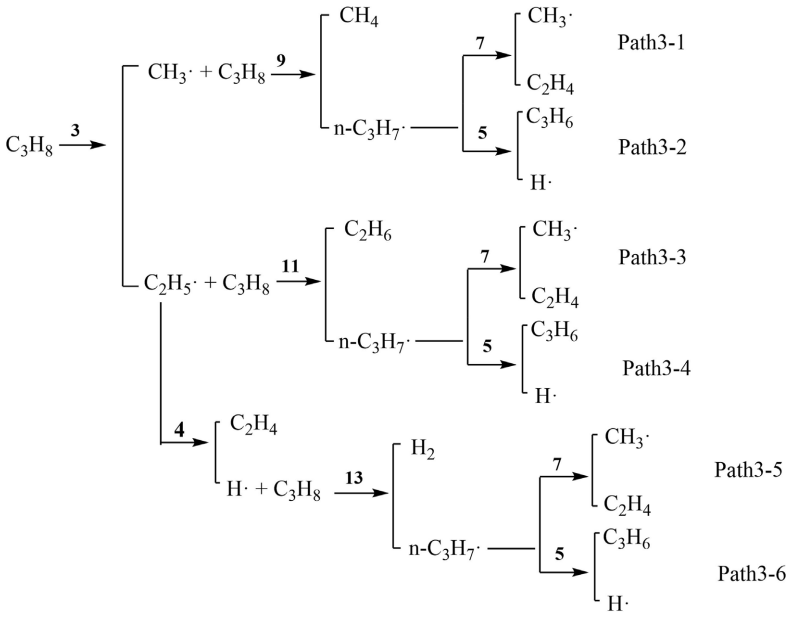

Figure 8. Design of propane pyrolysis path 3.

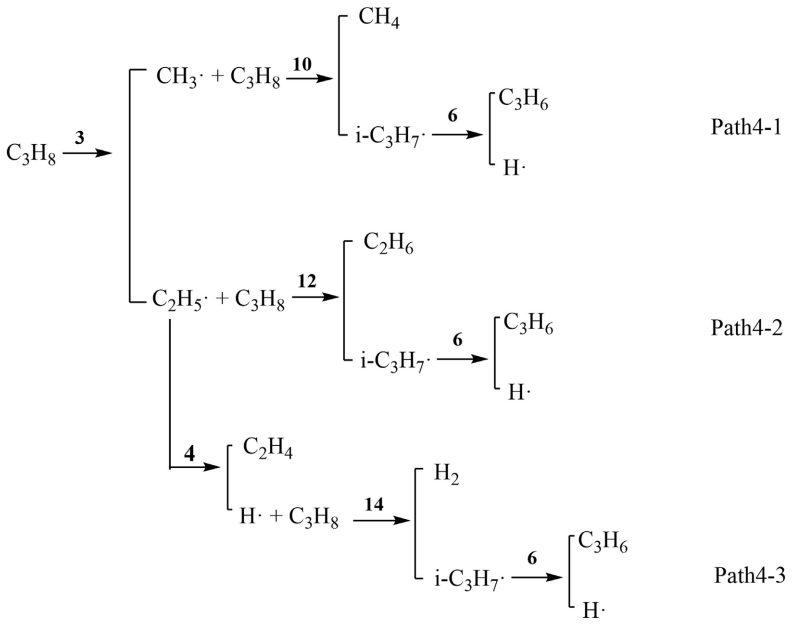

Figure 9. Design of propane pyrolysis path 4.

Hydrogen atom abstraction is the core step in radical chain propagation during gas-phase alkane pyrolysis. In pathway 3, radicals such as CH_3• and C_2H_5• generated from the initial C-C bond cleavage of propane abstract hydrogen atoms from

the secondary carbon (-CH_2) and primary carbon (-CH_3) sites of propane molecules within the system, converting them into *n*-C_3H_7• to sustain radical chain propagation. The secondary carbon hydrogen bond, possessing lower bond energy and higher electron density, becomes the preferred site for hydrogen abstraction. This mechanism directly determines the reaction priority for subsequent *β*-cleavage to produce products like CH_4 and C_2H_4. The primary sources of hydrogen atom abstraction are: 1) Unreacted propane molecules: The main hydrogen donor, from which radicals can abstract hydrogen from both secondary and primary carbon sites. Secondary carbon hydrogen, possessing lower bond energy and higher electron density, is the preferred abstraction site. 2) Reaction intermediates: Generated alkyl radicals such as *n*-C_3H_7• can also act as hydrogen donors in abstraction reactions, sustaining radical chain propagation. In the gas phase environment, molecular diffusion and high-frequency collisions provide ample contact opportunities for these abstraction reactions, ensuring the continuous advancement of the chain reaction.

The energy barrier diagrams for propane cracking pathways 3 and 4 are depicted in **Figure 10** and **Figure 11**, respectively, clearly illustrating the energy level differences between the respective reactions. Path 3 initiates with propane C-C bond cleavage, whose activation energy (95.59 kcal/mol) is lower than the C-H bond cleavages in Paths 1 and 2. This stems from the inherently weaker C-C bond energy compared to C-H bonds. In Path 3, the energy barrier for CH_4 (109.96 kcal/mol) is the lowest, as its formation relies on hydrogen abstraction and single-bond electron transfer, resulting in minimal energy consumption. In contrast, the barriers for ethylene (133.63, 137.55, 178.41 kcal/mol) and propylene (126.63, 130.55, 170.4 kcal/mol) are higher. This is because the *β*-cleavage of ethylene involves a C-C bond whose bond strength is enhanced by the electron density concentration effect from adjacent radicals, requiring higher energy input for cleavage. In contrast, the C-C bond corresponding to propylene experiences weaker electron density disturbance from radicals. Path 4's core radical is *i*-C_3H_7•. Its branched structure cannot undergo *β*-cleavage to form ethylene, thus yielding only propylene and alkane products. Its propylene formation energy barriers (132.26, 136.18, 177.03 kcal/mol) are higher than those in Path 3. This is because the hyperconjugation effect of the side chain disperses the electron cloud of the C-C bond, enhancing bond stability and increasing the fracture energy barrier. Conversely, the energy barrier for CH_4 in pathway 4 (107.74 kcal/mol) is lower than in pathway 3, as the side chain structure of *i*-C_3H_7• increases the electron cloud density at the hydrogen abstraction site, facilitating the abstraction reaction.

Regarding pyrolysis mechanisms, the C-C initiation fracture in Path 3 broadens the product spectrum. Low-energy hydrogen abstraction first drives alkane formation, followed by *β*-cleavage yielding alkenes. In contrast, the branched radical structure in Path 4 restricts the product range, clearly demonstrating the dual regulatory role of reactant bond properties and radical structure on pyrolysis energy barriers.

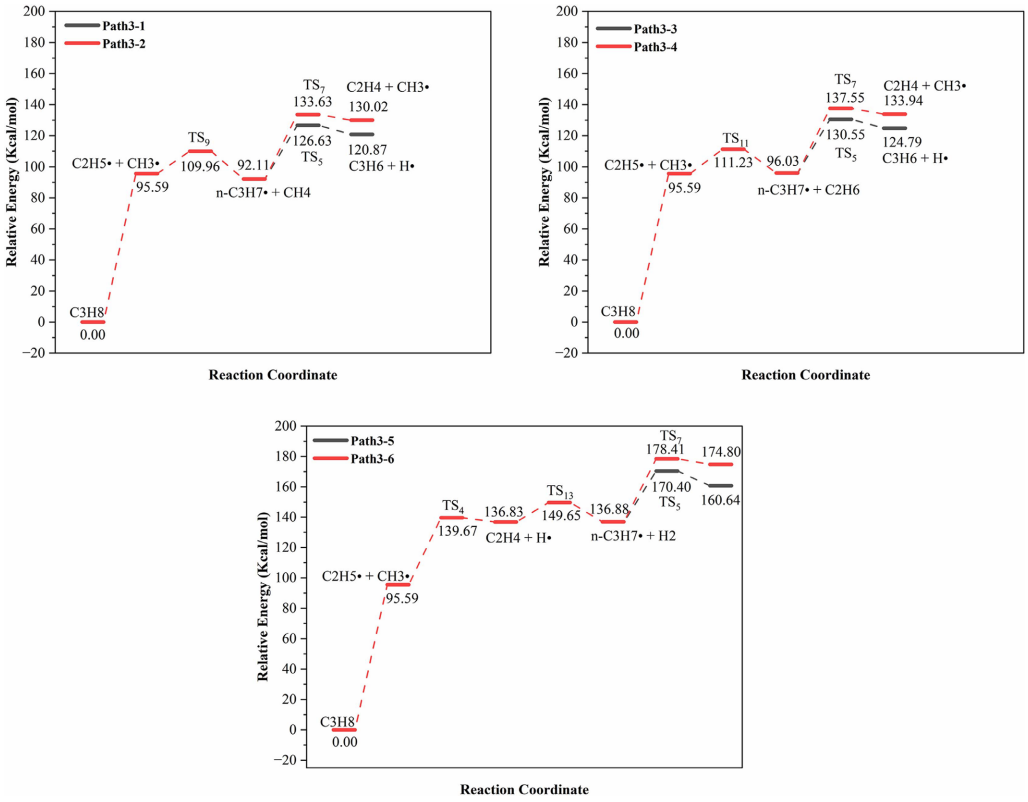

Figure 10. Schematic of the reaction energy barriers during the formation of ethylene and propylene in path 3.

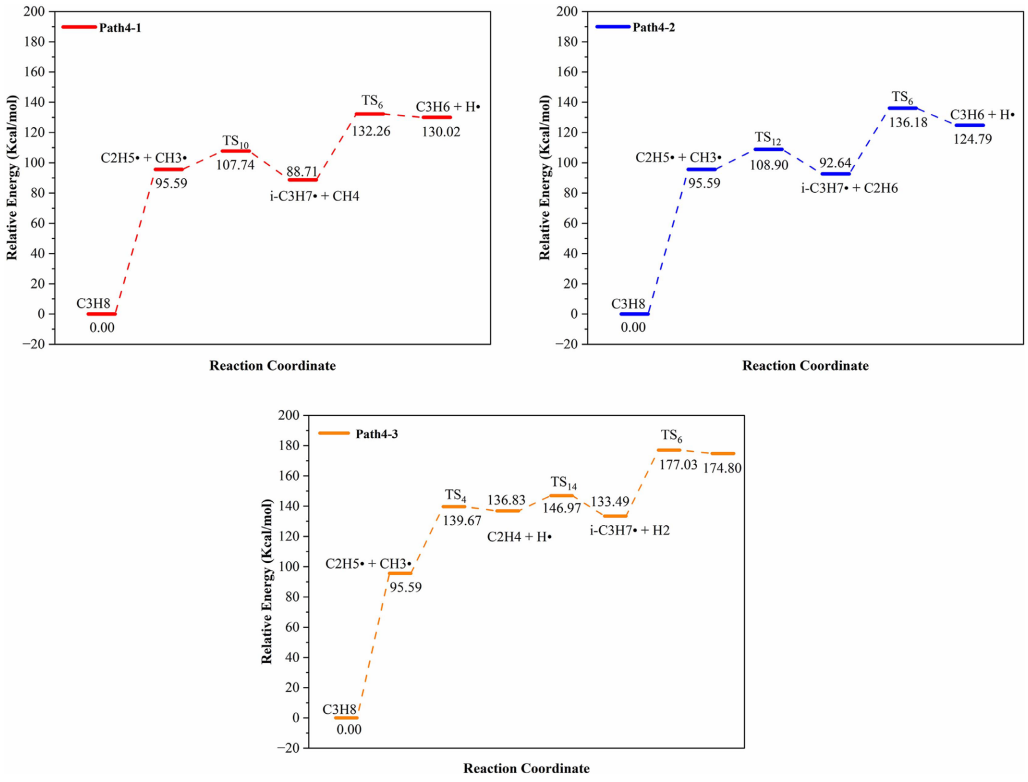

Figure 11. Schematic of reaction energy barriers during the formation of ethylene and propylene in Path 4.

In summary, based on the previously calculated bond dissociation energies, the initial activation energy barrier for C-C bond cleavage in propane molecules is lower than that for the C-H cleavage pathway. Pathways 3 and 4 emerge as critical pathways, primarily due to the synergistic effect between bond energy differences and reaction energy barriers. According to the Arrhenius equation, the lower activation energy corresponds to a higher reaction rate constant, enabling C-C initiation to dominate the kinetics during the early pyrolysis stage. Concurrently, the subsequent disproportionation/β-cleavage reactions of the C-C initiated propyl radical exhibit product selectivity: the activation energy for ethylene formation is significantly lower than that for propylene or methane pathways. This dual characteristic of "low initiation energy barrier + high product selectivity" directly determines ethylene's dominant position in the overall product composition, making it a core target for optimizing pyrolysis products.

4. Conclusions

This study focused on the core requirement of producing high-value-added olefins via propane pyrolysis. Using the M06-2X/6-31++G(d,p) method, we completed theoretical transition state calculations for all radical reactions involved in propane pyrolysis. Activation energies for key steps in the propane pyrolysis radical reaction network were calculated, and a dynamic energy barrier diagram was constructed. The study clarifies that the bond dissociation energy for C-C bonds in the initial propane reaction is lower than that for C-H bonds. The calculated initial reaction dissociation energy of propane C-C bond was 95.587 kcal/mol, and the dissociation energy of C-H bond was 108.069/104.672 kcal/mol. Based on this, four reaction pathways for ethylene and propylene formation were designed. Concurrently, it was discovered that the reaction energy barrier for ethylene formation is lower than that for propylene and other product pathways, establishing this as the core mechanism determining ethylene as the primary product. Finally, these findings provide atomic-scale theoretical foundations for controlling propane pyrolysis product distribution.

Given that this study focuses on resolving the atomic-scale mechanisms of propane pyrolysis, it has yet to overcome the limitations of traditional DFT computational scale and experimental validation depth. Future work will deepen research along two dimensions: "machine learning potential function+catalyst development". On one hand, training sets will be constructed based on the high-precision DFT data from this study to develop machine learning potential functions, enabling microsecond-scale simulations of million-level radical reaction networks and breaking through the limitations of traditional DFT computational scale. Second, by integrating dynamic energy barrier regulation mechanisms, we will design supported metal oxide catalysts that modulate transition state energy barriers through electronic interactions between active sites and radicals, thereby targeting enhanced propylene selectivity.

CRediT Authorship Contribution Statement

Methodology, Z. W., H. F. and R.-S. X.; Investigation, Z. W., H. F., M.-F. C. and Q.-F. Z; Conceptualization, H. F. and Q.-F. Z.; Writing-Original Draft Preparation, Z. W. and H. F.; Writing-Review & Editing, M.-F. C; Supervision, Q.-F. Z.

Data Availability

Data will be made available on request.

Acknowledgements

This study was partially supported by National Natural Science Foundation of China (grant no. 42271301).

Conflicts of Interest

The authors declare no conflicts of interest regarding the publication of this paper.

References

[1] Saito, H. and Sekine, Y. (2020) Catalytic Conversion of Ethane to Valuable Products through Non-Oxidative Dehydrogenation and Dehydroaromatization. *RSC Advances*, **10**, 21427-21453. https://doi.org/10.1039/d0ra03365k

[2] van Goethem, M.W.M., Barendregt, S., Grievink, J., Moulijn, J.A. and Verheijen, P.J.T. (2006) Ideal Chemical Conversion Concept for the Industrial Production of Ethene from Hydrocarbons. *Industrial & Engineering Chemistry Research*, **46**, 4045-4062. https://doi.org/10.1021/ie0609160

[3] Berreni, M. and Wang, M. (2011) Modelling and Dynamic Optimization of Thermal Cracking of Propane for Ethylene Manufacturing. *Computers & Chemical Engineering*, **35**, 2876-2885. https://doi.org/10.1016/j.compchemeng.2011.05.010

[4] Yang, M. and You, F. (2017) Comparative Techno-Economic and Environmental Analysis of Ethylene and Propylene Manufacturing from Wet Shale Gas and Naphtha. *Industrial & Engineering Chemistry Research*, **56**, 4038-4051. https://doi.org/10.1021/acs.iecr.7b00354

[5] Gerzeliev, I.M., Fairuzov, D.K., Gerzelieva, Z.I. and Maksimov, A.L. (2019) Production of Ethylene from Ethane Fraction by a Method Alternative to Steam Cracking. *Russian Journal of Applied Chemistry*, **92**, 1549-1557. https://doi.org/10.1134/s1070427219110120

[6] Gaffney, A.M. and Mason, O.M. (2017) Ethylene Production via Oxidative Dehydrogenation of Ethane Using M1 Catalyst. *Catalysis Today*, **285**, 159-165. https://doi.org/10.1016/j.cattod.2017.01.020

[7] Choudhary, V.R., Rane, V.H. and Rajput, A.M. (1998) Simultaneous Thermal Cracking and Oxidation of Propane to Propylene and Ethylene. *AIChE Journal*, **44**, 2293-2301. https://doi.org/10.1002/aic.690441018

[8] Deng, S., Li, H., Li, S. and Zhang, Y. (2007) Activity and Characterization of Modified Cr_2O_3/ZrO_2 Nano-Composite Catalysts for Oxidative Dehydrogenation of Ethane to Ethylene with CO_2. *Journal of Molecular Catalysis A*: *Chemical*, **268**, 169-175. https://doi.org/10.1016/j.molcata.2006.12.033

[9] Shi, X., Ji, S. and Wang, K. (2008) Oxidative Dehydrogenation of Ethane to Ethylene with Carbon Dioxide over Cr-Ce/SBA-15 Catalysts. *Catalysis Letters*, **125**, 331-339.

https://doi.org/10.1007/s10562-008-9569-3

[10] Abousrafa, A., Katebah, M.A., Linke, P. and Al-Rawashdeh, M. (2024) Piston Reactor for Chemical Energy Storage: Modeling Study to Explore Electro-Mechanical Conversion Route Using Propane Feedstock. *Chemical Engineering and Processing—Process Intensification*, **202**, Article ID: 109840. https://doi.org/10.1016/j.cep.2024.109840

[11] Mansfield, A. and Sophonrat, N. (2024) An Experimental and Modeling Study of Propane Oxidation Kinetics in Low Temperature Supercritical Water. *The Journal of Supercritical Fluids*, **214**, Article ID: 106392. https://doi.org/10.1016/j.supflu.2024.106392

[12] Hadadi, S.M., Alshamrani, K.M., Bajunaid, A.S. and Alosaimi, A.M. (2024) Production of Olefins by Dehydrogenation of Propane over Fe Modified ZSM-5. *OALib*, **11**, 1-10. https://doi.org/10.4236/oalib.1112358

[13] Zhang, H., Wang, J., Ma, C., Zhang, R., Wang, B., Zhang, Y., *et al.* (2025) Propane Dehydroaromatization on Ga-Modified HZSM-5 Catalyst: Brønsted/Lewis Acid Synergistic Effect. *Journal of Catalysis*, **447**, Article ID: 116147. https://doi.org/10.1016/j.jcat.2025.116147

[14] Zhang, D., Wang, S., Zhang, C., He, L. and Sun, W. (2024) Chemically Exfoliated Boron Nanosheets for Efficient Oxidative Dehydrogenation of Propane. *Nanoscale*, **16**, 1312-1319. https://doi.org/10.1039/d3nr05212e

[15] Salom-Català, A., Strugovshchikov, E., Kaźmierczak, K., Curulla-Ferré, D., Ricart, J.M. and Carbó, J.J. (2024) Reactive Force Field Development for Propane Dehydrogenation on Platinum Surfaces. *The Journal of Physical Chemistry C*, **128**, 2844-2855. https://doi.org/10.1021/acs.jpcc.3c07126

[16] Fan, Y., Gong, X., Liu, D., Li, X., Wang, X., Liu, Z., *et al.* (2024) A ReaxFF Molecular Dynamics Study of Pyrolysis Mechanism of Normal and Isomeric Decanes. *Proceedings of the* 2024 6*th International Conference on Civil Engineering, Environment Resources and Energy Materials* (*CCESEM* 2024), Guangzhou, 18-20 October 2024, 13-20. https://doi.org/10.2991/978-94-6463-606-2_3

[17] Liu, Z., Lu, A. and Wang, D. (2024) Deep Potential Molecular Dynamics Study of Propane Oxidative Dehydrogenation. *The Journal of Physical Chemistry A*, **128**, 1656-1664. https://doi.org/10.1021/acs.jpca.3c07859

[18] Patet, R.E., Caratzoulas, S. and Vlachos, D.G. (2016) Adsorption in Zeolites Using Mechanically Embedded ONIOM Clusters. *Physical Chemistry Chemical Physics*, **18**, 26094-26106. https://doi.org/10.1039/c6cp03266d

[19] Agrawal, K., Verma, A.M. and Kishore, N. (2019) DFT Investigation on Thermochemical Analyses of Conversion of Xylose to Linear Alkanes in Aqueous Phase. *Journal of Molecular Graphics and Modelling*, **90**, 199-209. https://doi.org/10.1016/j.jmgm.2019.05.005

[20] Guo, H., Tang, Y., Liu, S., Ma, Y., Fang, S., Curran, H.J., *et al.* (2023) Kinetic Properties Study of H Atom Abstraction by CH_3O_2 Radicals from Fuel Molecules with Different Functional Groups. *The Journal of Physical Chemistry A*, **127**, 1960-1974. https://doi.org/10.1021/acs.jpca.2c08100

[21] Liang, Y. and Lu, X. (2024) Theoretical Investigation on the H Atom Abstraction Reaction from C1-C4 Alkanes and Alkenes by NH_2 Radicals. *The Journal of Physical Chemistry A*, **128**, 3396-3407. https://doi.org/10.1021/acs.jpca.4c01229

[22] Rayne, S. and Forest, K. (2016) Performance of the Major Semiempirical, *Ab Initio*, and DFT Methods for Isomerization Enthalpies of Linear to Branched Heptanes. *Journal of Environmental Science and Health, Part A*, **51**, 583-587. https://doi.org/10.1080/10934529.2016.1141626

[23] Borrome, M. and Gronert, S. (2019) Gas-Phase Dehydrogenation of Alkanes: C-H Activation by a Graphene-Supported Nickel Single-Atom Catalyst Model. *Angewandte Chemie*, **131**, 15048-15052. https://doi.org/10.1002/ange.201907487

[24] Zhao, Y. and Truhlar, D.G. (2008) Density Functionals with Broad Applicability in Chemistry. *Accounts of Chemical Research*, **41**, 157-167. https://doi.org/10.1021/ar700111a

[25] Wu, H., Tang, R., Ren, X., Wang, M., Liang, G., Li, H., *et al.* (2025) Understanding Key Interactions between NO_x and C_2-C_5 Alkanes and Alkenes: The *Ab Initio* Kinetics and Influences of H-Atom Abstractions by NO_2. *Combustion and Flame*, **272**, 113885. https://doi.org/10.1016/j.combustflame.2024.113885

[26] Wiberg, K.B. (2012) Accuracy of Calculations of Heats of Reduction/Hydrogenation: Application to Some Small Ring Systems. *The Journal of Organic Chemistry*, **77**, 10393-10398. https://doi.org/10.1021/jo302118b

[27] Wu, Y., Tao, R., Li, B., Hu, C., Zhang, W., Yuan, H., *et al.* (2024) New Insights into Brominated Epoxy Resin Type WPCBs Pyrolysis Mechanisms: Integrated Experimental and DFT Simulation Studies. *Science of the Total Environment*, **912**, Article ID: 169610. https://doi.org/10.1016/j.scitotenv.2023.169610

[28] Wu, J., Ning, H., Ma, L. and Ren, W. (2018) Accurate Prediction of Bond Dissociation Energies of Large N-Alkanes Using ONIOM-CCSD(T)/CBS Methods. *Chemical Physics Letters*, **699**, 139-145. https://doi.org/10.1016/j.cplett.2018.03.041

[29] Blanksby, S.J. and Ellison, G.B. (2003) Bond Dissociation Energies of Organic Molecules. *Accounts of Chemical Research*, **36**, 255-263. https://doi.org/10.1021/ar020230d

[30] Baş, E.E., Karahan, S., Köstereli, Z., Haktanır, M. and Aviyente, V. (2020) Pyrolysis of Alkanes: A Computational Approach. *The Journal of Physical Chemistry A*, **124**, 5700-5708. https://doi.org/10.1021/acs.jpca.0c02858

[31] Conrad, J.K., Anderson, K., Sosulin, I.S., Wilbanks, J.R., Klaehn, J.R., Pilgrim, C.D., *et al.* (2025) Radiation-Induced Chemical Yields of Carbon-Centered Radicals and Hydrogen Atoms from the γ Irradiation of *n*-Dodecane. *The Journal of Physical Chemistry A*, **129**, 10496-10506. https://doi.org/10.1021/acs.jpca.5c06414

[32] Montgomery, J.A. and Petersson, G.A. (1990) On the C-H Bond Dissociation Energy of Acetylene. *Chemical Physics Letters*, **168**, 75-78. https://doi.org/10.1016/0009-2614(90)85105-l

[33] Kang, J., Ran, J., Niu, J., Shi, J., He, J. and Yang, Z. (2019) Experimental and Theoretical Study on Propane Pyrolysis to Produce Gas and Soot. *International Journal of Hydrogen Energy*, **44**, 22904-22918. https://doi.org/10.1016/j.ijhydene.2019.06.214

[34] Cassady, S.J., Choudhary, R., Boddapati, V., Pinkowski, N.H., Davidson, D.F. and Hanson, R.K. (2020) The Pyrolysis of Propane. *International Journal of Chemical Kinetics*, **52**, 725-738. https://doi.org/10.1002/kin.21395

[35] Qi, C., Ding, J., Wang, Y., Ning, Y., Wang, Y., Liang, H., *et al.* (2023) Investigation of the Upper Flammability Limit of Ethylene/Propane Mixtures in Air at High Temperatures and Pressures. *Energy*, **281**, Article ID: 128114. https://doi.org/10.1016/j.energy.2023.128114

[36] Lehrle, R.S., Peakman, R.E. and Robb, J.C. (1982) Pyrolysis-Gas-Liquid-Chromatography Utilised for a Kinetic Study of the Mechanisms of Initiation and Termination in the Thermal Degradation of Polystyrene. *European Polymer Journal*, **18**, 517-529. https://doi.org/10.1016/0014-3057(82)90054-4